Earth and Planetary Science Letters 301 (2011) 444–456

Contents lists available at ScienceDirect

Earth and Planetary Science Letters

journal homepage: www.elsevier.com/locate/epsl

Characterization of Navajo Sandstone concretions: Mars comparison and criteria for distinguishing diagenetic origins

Sally L Potter [a,*], Marjorie A. Chan [a], Erich U. Petersen [a], M. Darby Dyar [b], Elizabeth Sklute [b,1]

[a] University of Utah, Department of Geology and Geophysics, 115S. 1460E. Rm. 383, Salt Lake City, UT 84112, United States
[b] Mount Holyoke College, Department of Astronomy, 50 College Street, South Hadley, MA 01075, United States

ARTICLE INFO

Article history:
Received 1 June 2010
Received in revised form 14 November 2010
Accepted 16 November 2010
Available online 18 December 2010

Edited by: P. DeMenocal

Keywords:
Navajo Sandstone
concretions
Mars
diagenesis
iron oxide
Meridiani Planum

ABSTRACT

The eolian Jurassic Navajo Sandstone spheroidal hydrous ferric oxide (HFO) concretions are divided into two size classes: macro-concretions of >5 mm diameter and micro-concretions of <5 mm diameter. Three internal structural end-members of macro-concretions are described as rind, layered, and solid. Two end-members of micro-concretions are rind and solid.

Chemical and mineralogical gradients (μm- to mm-scale) are identified with QEMSCAN (Quantitative Elemental Mineralogy using a SCANning electron microscope) and visible to near infrared (VNIR) reflectance spectroscopy. Three HFO phases are identified using VNIR reflectance spectroscopy.

i. An amorphous HFO phase is typically located in the rinds.
ii. Goethite is present along interior edges of rinds and throughout the interiors of layered and solid concretions.
iii. Hematite is present in the centers of rind concretions.

A synthesis of petrographic, mineralogical and chemical analyses suggests that concretions grow pervasively (as opposed to radially expanding). Our model proposes that concretions precipitate initially as an amorphous HFO that sets the radius and retains some original porosity. Subsequent precipitation fills remaining pore space with younger mineral phases. Inward digitate cement crystal growth corroborates concretion growth from a set radius toward the centers. Internal structure is modified during late stage precipitation that diffuses reactants through semi-permeable rinds and overprints the interiors with younger cements.

Physical characterization of textures and minerals provides diagnostic criteria for understanding how similar concretions ("blueberries") form in Meridiani Planum, Mars. The analogous Navajo Sandstone concretions show similar characteristics of *in situ* self-organized spacing, spheroidal geometries, internal structures, conjoined forms, and precursor HFO phases that dehydrate to goethite or hematite. These characteristics indicate a common origin via groundwater diagenesis.

1. Introduction

The eolian Jurassic Navajo Sandstone is widely exposed throughout southern Utah and northern Arizona and is the largest erg that exists on modern or ancient Earth (Blakey, 1994; Blakey et al., 1988). The unit is renowned for its dramatic color patterns resulting from iron precipitation throughout its burial history (Beitler, 2003, 2005; Bowen et al., 2007; Chan et al., 2000, 2004, 2005; Parry et al., 2004; Seiler, 2008). The Spencer Flat study area located in Grand Staircase Escalante National Monument (GSENM; Fig. 1A,B in supplementary material) hosts a variety of hydrous ferric oxide (HFO) precipitation geometries (Fig. 1C in supplementary material).

A tripartite geochemical fluid flow model (Chan et al., 2000, 2005) describes the iron source–mobilization–precipitation cycle that is reflected in a variety of concretionary geometries and diagenetic facies (mappable geochemical facies based on color).

i. Iron source: Fe^{3+} precipitated as early diagenetic grain coatings from the breakdown of detrital ferromagnesian minerals.
ii. Iron mobilization: A reducing fluid infiltrated the sandstone and mobilized the iron into solution as Fe^{2+}.
iii. Iron precipitation: When this iron-bearing, reducing fluid met and mixed with an oxidizing fluid, Fe^{3+} precipitated as HFO cements.

The purpose of this study is to characterize the physical and chemical attributes of concretions including external features (concretion shape, size and texture) as well as the internal structure, cement texture, mineralogy and diagenetic phases. Although

* Corresponding author.
E-mail address: sally.potter@utah.edu (S.L. Potter).
[1] Now at Department of Geosciences, Stony Brook University, Stony Brook, NY 11794-2100, United States.

0012-821X/$ – see front matter © 2010 Elsevier B.V. All rights reserved.
doi:10.1016/j.epsl.2010.11.027

diagenetic iron precipitation in the Navajo Sandstone has been well studied (e.g., Beitler, 2005; Chan et al., 2000; Seiler, 2008), genetic models for spheroidal concretions warrant further investigation. This synthesis of characteristics is used to interpret how HFO concretions form and how diagenetic processes affect concretions throughout the groundwater history of the sandstone.

Navajo Sandstone concretions have been proposed as a terrestrial analog for Burns formation spherules in Meridiani Planum, Mars (Chan et al., 2004; Ormo et al., 2004); however, a debate still ensues as to whether this example represents a good analog, particularly geochemically (Morris et al., 2005; Squyres and Knoll, 2005). Detailed characterization of the Navajo Sandstone concretions is clearly required and has not been done previously. The diagnostic features of Navajo Sandstone diagenetic concretions are compared herein with Mars spherules to constrain diagenetic origin.

1.1. Concretion growth

The most common and best studied concretions are carbonate precipitates (e.g., Clifton, 1957; Coleman and Raiswell, 1981, 1995; Lyons et al., 2007; Mozley and Davis, 2005; Raiswell, 1976; Raiswell et al., 2000; Seilacher, 2001). Two end-member genetic models for carbonate concretions proposed by Raiswell et al. (2000) are concentric growth and pervasive growth (Fig. 2 in supplementary material). Their terminology is used in this paper to describe HFO concretions, although it should be noted that the exact nucleation mechanisms for carbonate concretions in mudrocks may not be directly applicable to iron oxide concretions in sandstones.

Concentric growth occurs when a small piece of organic matter biogenically nucleates the precipitation reaction. The concretions grow radially with an increasing radius. Pervasive growth occurs as the crystals nucleate and grow concurrently throughout the body of the concretion. Pervasive growth is particularly common in siderite (iron carbonate) concretions (Mozley and Davis, 2005; Raiswell et al., 2000; Seilacher, 2001). Pervasive growth concretions initially develop as plastic, porous, weakly cemented masses that become more rigid with further cementation (Raiswell et al., 2000).

In carbonates, cement textures are diagnostic of the type of concretion growth. Multiple generations of cements (isopachous cements within pore spaces) indicate pervasive growth (Feistner, 1989; Mozley, 1989; Raiswell et al., 2000; Seilacher, 2001). In these pervasive growth concretions, early cementation forms a framework with some small, retained porosity so that late stage pore filling can occur (Dickson and Barber, 1976; Hudson, 1978; Huggett, 1994; Jordan et al., 1992; Raiswell et al., 2000).

The rate of concretion formation is difficult to determine. Estimates range from 65 million years in pyrite concretions (Prosser et al., 1994) to between 140,000 and 65 million years in septarian calcite nodules (Boles et al., 1985) to 7500–20,000 years in Quaternary calcareous concretions (Pantin, 1958). Research on modern iron oxide concretions in acid saline lakes (Western Australia) suggest concretions can form within hundreds of years at low temperature in acidic conditions (Bowen et al., 2008). Lab experiments in agarose gels with concentrated chemicals nucleate concretions within a matter of days at room temperature (Barge and Petruska, 2007). Other modeling experiments of diffusion rates based on early Mars conditions suggest that concretion growth occurs on the scale of thousands of years (Sefton-Nash and Catling, 2008).

2. Methods

2.1. Field methods

Concretions were examined throughout the ~120 km^2 Spencer Flat area and macroscopic characteristics such as size, internal/external structures and geometry were documented. Exterior and interior colors of concretions were described using the Munsell Rock-Color Chart (1975). Representative samples of typical and atypical concretions were collected for laboratory analyses from loose populations of concretions.

Size diameters of 1300 concretions at eight sites were measured along the longest axis using a digital caliper to document representative size populations and for comparison with size data for Mars concretions. Measurements are accurate within 0.01 mm.

2.2. Lab measurements

2.2.1. Petrography

Thin sections from 90 concretion samples (1 to 10 cm in diameter) represent the range of internal structures (rind, layered and solid). These were examined petrographically to document cement textures. Thin sections of six host rock samples comprise a reference for comparison with concretions.

2.2.2. QEMSCAN

QEMSCAN (Quantitative Elemental Mineralogy using a SCANning electron microscope) is a set of four high-speed energy dispersive detectors that produce a detailed mineralogical image of a polished thin section or plug. QEMSCAN can distinguish variations in cement mineralogy, chemistry and texture that allow inference of chemical gradients and mineralogical zonation across the concretions. QEMSCAN can also image porosity and give the area percentage of any mineral phase or porosity in two dimensions. QEMSCAN is built by Intellection and the instrument used for this study is located at Xstrata Nickel in Sudbury, Ontario.

Polished thin sections were made of five representative concretion samples. A Species Identification Protocol (SIP) was developed for this sample set. Mineralogical images of each entire thin section were made at 10 μm pixel-spacing. Detailed examinations within the rinds and interiors were made at 1 μm pixel-spacing. Back scattered electron (BSE) images of the five samples were examined in conjunction with QEMSCAN to compare textural properties with different mineral phases.

2.2.3. Visible to near infrared (VNIR) reflectance spectroscopy

VNIR reflectance spectroscopy is an effective method for determining iron and clay mineral phases of cements in the Navajo Sandstone (Bowen et al., 2007; Seiler, 2008) because the framework grains (quartz and feldspar) do not have distinct absorption features in the visible to near infrared (350–2500 nm) range but the HFOs and clay minerals do. An ASD FieldSpec Pro was used to obtained spectra on 22 samples (15 samples of rind concretions, 5 samples of layered concretions and 2 samples of solid concretions). Spectra could only be obtained for two solid concretions because insufficient light is reflected from dark concretions.

Concretions were prepared by cutting or breaking them in half. The fiber optic cable of the unit was positioned ~9 mm from the sample in order to obtain a 3 mm diameter field of view. Spectra were acquired in transects across the samples in overlapping intervals. The spectra were graphed and absorption features were compared with standards from the USGS spectral library 06a (Clark et al., 2007).

3. Textural and geometric characterization

3.1. Macro-concretions

Macro-concretions are spheroids preferentially cemented with HFO and defined as >5 mm in diameter (see Table 1 for a summary of textural and geometric concretion characterization). Macro-concretions are further divided into three categories based on internal structural end-members: rind, layered, and solid (Fig. 1A,B,C). They

Table 1
Navajo Sandstone HFO concretion characterization summary.

	DESCRIPTION	INTERPRETATION
MACRO	> 5 mm in diameter	
INTERIOR STRUCTURE		
Rind	1-10mm well-cemented, hollow spheroid with interior depleted of cement	• Interior structure varies between end members
Layered	Well-cemented, concentric layers throughout interior	• Form by diffusion • Faster diffusion and/or advection
Solid	Evenly cemented with HFO throughout entire concretion; >5 mm diameter	transports more reactants → larger sizes
MICRO	< 5 mm in diameter	
INTERIOR STRUCTURE		
Rind Solid	Solid interiors more common	Form by diffusion
SIZE		
Range	0.8 mm to 8+ cm diameter	Size ranges indicate reaction fronts
Mean	22.46 mm diameter	with varying reactant supply
Distribution	• macros: 5-12 mm and >12 mm • Micros: <5 mm diameter	
GEOMETRY		
Aspect ratio Range: 1.00-1.97; mean=1.10; median=1.06		• Diffusion + advection
	• Perfectly spherical (aspect ratio=1.00) • Nearly spherical (aspect ratio ≤1.06) • Discoidal (aspect ratio >1.06)	• Faster diffusion/ advection →more reactants →larger sizes • Faster diffusion rates along
Location	• Nearly spherical →massive host rock • Discoidal concretions → grain flow laminae	permeable lamina →discoidal
EXTERIOR STRUCTURE		
Color	black or brown	Mineralogy and crystal size
Texture	Smooth and shiny	Weathering, desert varnish
	Rough and sandy	Not as densely cemented
	Bumpy "avocado skin" texture	• Micros nucleate on macros • Radial growth component
CEMENT (MICROSCOPY)		
Rind		
rind	Three isopachous textural phases	• Pervasive growth
interior	Kaolinite blebs, some illite grains coatings, granular HFO	• Interiors depleted of cement
Layerd		
rind	Rind similar to rind concretions	Pervasive growth
interior	Fine-grained, granular HFO in layers, kaolinite in blebs	
Solid	Granular HFO throughout	radial + pervasive growth
MINERALOGY (QEMSCAN)		
Rind		
rind	• Smooth textured HFO (95%) • Frothy textured HFO (2%) • Kaolinite (2%) • MnO (0.2%) • Porosity (2%)	Late-stage MnO pore fill.
interior	• Smooth textured HFO (20%) • Frothy textured HFO (27%) • Kaolinite (50%) • Porosity (29%)	
MINERALOGY (Vnir SPECTROSCOPY		
Rind		
rind	Amorphous HFO/goethite	• Concretions initially precipitate as
interior	• Goethite near outer edge • Hematite in center	rind structure • Late-stage mineralization events
Layered	• Amorphous HFO/goethite • Hematite in depleted center	alter internal structure
Solid	Amorphous HFO/goethite	

are present both *in situ* and weathered out and collected in topographic lows throughout Spencer Flat. *In situ* macro-concretions exhibit a geochemically self-organized spacing rather than a random spacing (Potter and Chan, submitted for publication).

Concretion exteriors are typically either dark-colored or light-colored (see Supplemental section for Munsell color descriptions). Interior colors are a range of red, yellow or brown colors. Dark-colored concretions are typically well-cemented. When weathered out and

Fig. 1. Navajo Sandstone macro-concretions. Large tick marks on scale bar are cm. A. Rind macro concretion end member with well-cemented rind surrounding interior relatively depleted of HFO cement. B. Layered macro concretion end member with HFO cemented layers throughout the interior. C. Solid macro concretion end members evenly cemented with HFO throughout the concretion. D. Range of exteriors: light colored, sandy and rough or dark colored, smooth and polished (see text for Munsell color descriptions). E. Bumpy "avocado skin" exterior of coalesced micro-concretions. F. Spheroidal and discoidal concretions. Spheroidal concretions are present in more homogenous sandstone. Where sandstone is differentiated due to grain size contrast, discoidal concretions are present. G. Some of the varieties of interiors that blend end members between rind, layered and solid. H. Layered macro concretion with a friable center depleted of HFO cement. I. Atypical interiors that are better cemented than rinds or layers.

loose, they may exhibit a shiny, smooth polish (Fig. 1D). Some light-colored concretions are well-cemented, but have a sandy exterior and do not exhibit a high polish (Fig. 1D). Some exteriors exhibit a bumpy, "avocado-skin" texture (Fig. 1E).

Geometries of macro-concretions range from spherical (aspect ratio = 1) to nearly spherical (aspect ratio ≤ 1.06) to discoidal (aspect ratio > 1.06) depending on anisotropies in the host rock (Potter and Chan, submitted for publication) (Fig. 1F). In general, the spheroidal macro-concretions occur in the upper portion of the Navajo Sandstone where much of the cross bedding is disturbed by soft sediment deformation and/or where the sandstone is massive. In the lower Navajo Sandstone where cross bedding is more prevalent and undisturbed, concretions are either spheroidal (within thick grainflow beds) or discoidal where concretions grow in alternating wind ripple and grainflow laminae. Discoidal growth is typically elongate along the more permeable grainflow laminae.

3.1.1. Rind end-member

Rind concretions are the most common type of macro-concretion present in Spencer Flat. They are typified by a thin (1 mm to 10 mm) spheroidal rind consisting of HFO cemented sandstone surrounding an interior that is relatively depleted of cement (Fig. 1A). Rind concretions are generally preferentially cemented relative to the surrounding host rock and weather out to collect in topographic lows (Fig. 1C in supplemental section). Rinds typically comprise ~25–60% of concretion volume, estimated by subtracting the volume of the interior from the total volume of the concretion and assuming perfect sphericity. Interiors of the rind concretion end-members are friable relative to the rind (Fig. 1A). However, they display varying degrees of cementation and commonly contain asymmetrical or concentric red, brown or yellow rings in banded patterns (Liesegang bands; Fig. 1G).

3.1.2. Layered end-member

Layered macro-concretions have exterior rinds similar to those of rind macro-concretions but also exhibit preferentially cemented, thin, overlapping layers (~0.3–1 mm thick) that persist throughout the interior of the concretion (Fig. 1B). Layered concretions have approximately 2–15 layers depending on the diameter of the concretion. These layers extend throughout the entire interior of the concretion or the concretion may have a center depleted of cement similar to rind concretions (Fig. 1H). The layers resemble Liesegang bands that are common in the interiors of rind concretions, but they are better cemented and are a darker color.

3.1.3. Solid end-member

Solid macro-concretions (Fig. 1C) are evenly cemented with HFO throughout the entire concretion. Solid concretions may have a rind that is slightly differentiated from the interior by color, but the interior is not depleted of HFO cement. Some solid interiors are preferentially harder than the rinds (Fig. 1I).

3.1.4. Interpretation

External color differences result from factors such as degree of cementation, different cement crystal sizes and/or different mineral phases. For instance, hematite crystals larger than 5 μm are grey and crystals smaller than 5 μm are reddish-brown (Glotch et al., 2004; Lane et al., 1999); goethite tends to be yellow or brown.

External textural differences also result from a variety of factors. Smooth, shiny exteriors occur only on weathered out concretions and

could be due to weathering (sandblasting) or a desert varnish. Bumpy external texture results from micro-concretions coalescing to form larger macro-concretions and may contribute a component of radial growth to "avocado skin" macro-concretions. This likely occurs by Ostwald ripening because smaller concretions nucleate more easily than larger concretions and nucleate preferentially where HFO is already precipitated (see Steefel and Van Cappellen, 1990, for a discussion of Ostwald ripening).

Concretion geometry results from complex interactions between diffusive and advective mass transfer (Potter and Chan, submitted for publication). Nearly spherical concretions imply even growth in isotropic media by diffusive mass transfer because homogenized host rock evenly distributes diffusion rates (McBride et al., 2003; Mozley and Davis, 2005; Seilacher, 2001). Therefore, macro-concretions formed in diffusive reaction fronts. However, advection may have a role in mobilizing larger amounts of reactants to these diffusive reaction fronts and thereby forming larger size populations. Where cross bedded sandstone has alternating grainflow and wind ripple laminae, concretions are discoidal due to faster diffusion rates along the more porous and permeable grainflow laminae.

Layered macro-concretions occur in reaction fronts with rind and solid macro-concretions and are indistinguishable by external appearance from these other end-members. These characteristics imply a similar initial genesis for all end-members of macro-concretions. The presence of rinds in layered and solid end-members suggests that concretions likely precipitate initially as rind concretions and internal structures are modified during subsequent precipitation events.

The layered end-member interiors consist of periodic precipitation bands (Liesegang bands) that can persist throughout the interior of the concretion. Liesegang bands form via diffusive reactant transfer (Ortoleva, 1994). Therefore, the internal layers indicate inward directional diffusion and interiors are likely modified as additional reactants (iron and/or oxygen) diffuse through outer rinds during late stage precipitation. Another possible explanation for late stage modification of interior structure is that reactants are drawn from interior sources and/or edges of the rinds and reprecipitate throughout the interiors; however, textural analysis of cements and inward digitate cement growth suggest that diffusion of reactants through gel-like rinds is more likely (Raiswell et al., 2000).

3.2. Micro-concretions

Micro-concretions (Fig. 2A) are more common than other types of concretions in the Navajo Sandstone and are ubiquitous throughout southern Utah and northern Arizona. Micro-concretions are typically present where regional secondary diagenetic facies have precipitated. Micro-concretions are generally cemented well enough to weather out of the host rock and collect in topographic lows; however, they do exhibit varying degrees of cementation. *In situ* micro-concretions typically exhibit a geochemically self-organized spacing (Potter and Chan, submitted for publication) and some occur between Liesegang bands (Fig. 2B). Micro-concretions also appear coalesced to form thicker rinds of macro-concretions creating the bumpy external appearance resembling avocado skin on some macro-concretions (Figs. 1E and 2C).

Diffusive reaction fronts in the Navajo Sandstone are associated with diagnostic features such as Liesegang bands (Beitler, 2005; Eichhubl et al., 2004; Potter and Chan, submitted for publication; Seiler, 2008). Spheroidal geometry is also indicative of diffusive mass transfer (McBride et al., 2003; Mozley and Davis, 2005; Seilacher, 2001). Therefore, the ubiquitous nature of spheroidal micro-concretions, their association with Liesegang bands, and their spheroidal geometry suggest that micro-concretions form via simple diffusion.

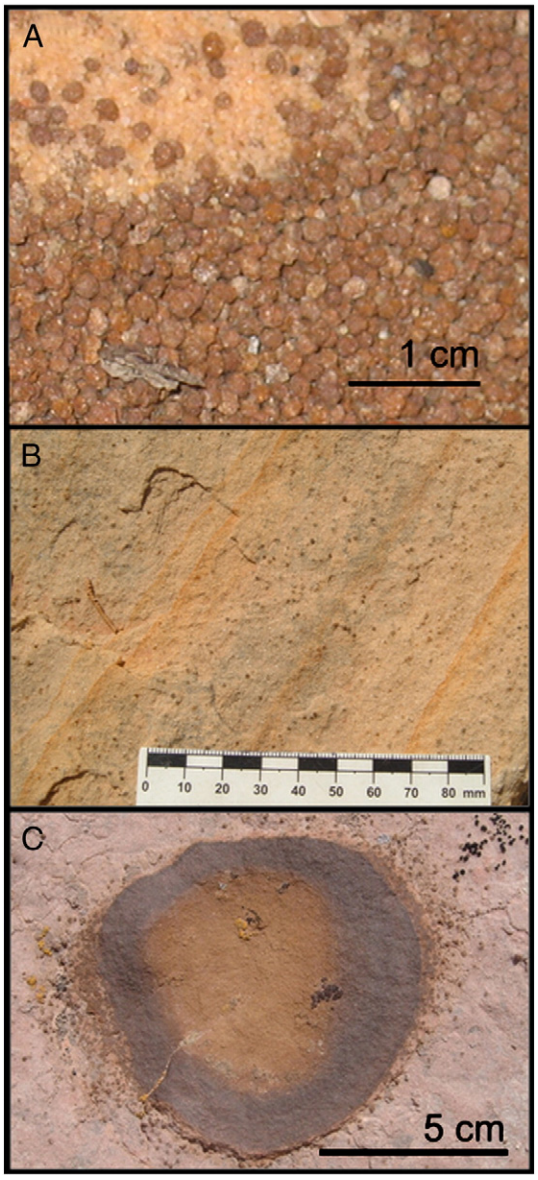

Fig. 2. Micro-concretions. A. Loose micro-concretions collected in topographic low. B. Micro-concretions between Liesegang bands in a diffusive reaction front. C. Micro-concretions coalescing to form larger concretion.

3.3. Doublets and triplets

Doublets and triplets typically consist of equal-sized, conjoined concretions. Both macro and micro-concretions can form doublets and triplets and conjoined forms are present both *in situ* and loose (Fig. 3A). Doublets and triplets comprise ~5% or less of a typical loose collection where most of the concretions are single forms; however, one reaction front (~0.25 km^2) in the study area contains ~95% macro concretion doublets (ranging from ~1 to 4 cm diameter for each side; Fig. 3A). *In situ* doublets and triplets in both types of reaction fronts (fronts that produce mostly single forms and fronts that produce mostly doublets) typically exhibit self-organized spacing as do other spheroidal concretions.

Exterior structure of conjoined forms is similar to single macro-concretions; exteriors can be smooth and polished or sandy (Fig. 3A, B). Some exteriors are bumpy ("avocado skin") from coalesced micro-concretions (Fig. 3B). Interior structure of conjoined forms ranges between rind, layered and solid end-members (Fig. 3C,D). All

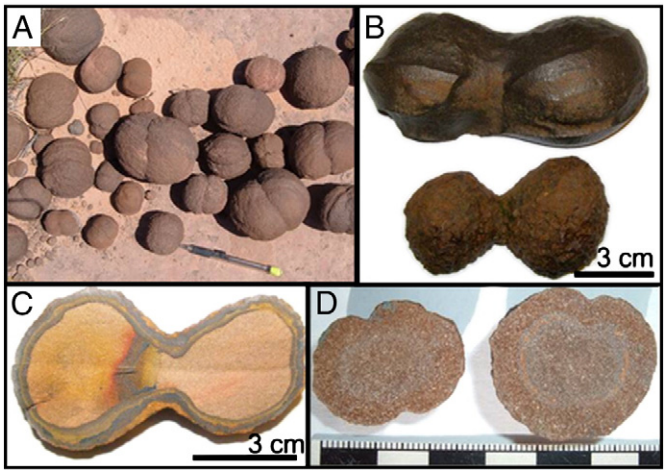

Fig. 3. Doublets. A. Loose doublets from reaction front with mostly fused forms. Note the range of sizes (pencil for scale). B. Doublets with smooth (top) and "avocado skin" (bottom) exterior structure. C. Layered doublet with interior depleted of cement. Doublets share internal structure. D. Solid interior structure with faint rind defined by color difference. Large tick marks on scale bar = cm.

conjoined forms typically share internal structure (Fig. 3C,D); they are not discrete, fused concretions.

Other multiple conjoined forms (i.e., clumped clusters of more than three spheroidal concretions) are not as common as the other single, double or triple forms. These clusters form in localized reaction fronts (1–2 m^2) and result from a nucleation pattern that produces clusters instead of a geochemically self-organized spacing (Potter and Chan, submitted for publication).

The equality of size for each conjoined section, the local abundance in one reaction front and the shared internal structure all indicate that doublets and triplets likely form in one precipitation event where two (or three) conjoined concretions nucleate simultaneously. If a single concretion formed and a second was added in a subsequent precipitation event, the two fused concretions would likely be unequal in size and would share a dividing center rind between them.

3.4. Size distribution

Three concretion size populations are recorded in Spencer Flat (Fig. 4). Here we differentiate between macro-concretions (>5 mm diameter) and micro-concretions (<5 mm diameter), but there is a natural division in the macro concretion population of two size populations (5–12 mm and >12 mm). Descriptive statistics for the <5 mm and the >12 mm size populations show a skewness <1, indicating normal distributions. The 5–12 mm population has a skewness ~1, indicating a nearly normal distribution. Although the three size ranges likely overlap and smaller populations may be included in these size ranges, the small skewness of the three populations suggests a primarily trimodal distribution for the entire range of sizes measured in Spencer Flat. For all loose concretions (n = 1300), diameters range from 0.94 mm to 81.79 mm with a mean diameter of 22.46 mm, a median diameter of 21.65 mm and a standard deviation of 15.70 mm.

A typical accumulation of loose concretions in a topographically low area (1–2 m^2) contains >1 size population and these accumulations are a result of resistant concretions forming a "let down" lag as the host rock erodes. These lags represent 10s of meters of eroded section. More than one size population in a loose accumulation represents overlapping reaction fronts that nucleate similar sizes and/or geometries because two or more size populations can be present *in situ*.

Reactant supply is controlled by diffusive and advective mass transfer processes and varying diffusion rates; therefore, different size populations represent discrete reaction fronts with varying reactant supply. Size of reaction fronts is difficult to determine; however, a reaction front that produced mostly doublets extends ~0.25 km^2. A larger reaction front (~0.6 km^2) is also recognized by a population of "avocado skin" macro-concretions. The abundance and localization of macro-concretions throughout Spencer Flat suggest that a reaction front of these ~2–3 cm size concretions may be significantly larger (up to 120 km^2). The 2–3 cm size population may have formed in numerous divided reaction fronts; however, the presence of two or more size ranges *in situ* throughout Spencer Flat combined with evidence for multiple precipitation events (Potter and Chan, submitted for publication) suggests that reaction fronts nucleate specific size ranges.

4. Analytical results

4.1. Petrography

In the outer layer of rind concretions, HFO cementation nearly occludes pore space, yet in the interiors, HFO cementation is sparse (Fig. 5A). The interior edges of the rinds are irregularly shaped and exhibit inward digitate growths toward the center of concretions (Fig. 5A).

In the rinds of macro-concretions (rind and layered end-members), three textures of HFO cement are distinguished through petrographic microscopy: i. granular-textured cement coats and rims the grains, ii. tabular cement is adjacent to the granular cement and radiates into the pore space, and iii. late stage pore filling consists of small, euhedral crystals (Fig. 5B). Rinds of layered concretions have the same three textural phases of HFO cement; however, the interior layers (Fig. 5C) are composed solely of a fine-grained phase. In solid concretions, the HFO cement is granular-textured (Fig. 5D).

Cement in the depleted interiors is primarily kaolinite occurring in blebs that are independent of orthoclase grains. HFO is present in minor amounts in the interiors in pore throats and as grain coatings and is granular-textured (Fig. 5E). Many grains exhibit a thin illite coating (Fig. 5F).

Only two samples out of 90 contained euhedral HFO after pyrite pseudomorphs visible with a reflected light microscope. No other HFO replacement pseudomorphs (such as siderite) were observed.

4.2. QEMSCAN

Cements in the rind areas of concretions are ~27% HFO; cements in the interiors are 2% kaolinite and 0.5% HFO (including framework grains and porosity). Well-cemented rinds are of low porosity (~2%) and friable interiors are of high porosity (~29%). After normalization to exclude framework grains and porosity, rind cement is composed of 96% HFO and 2% kaolinite. The interior cement is 50% kaolinite and 47% HFO. Manganese oxide (MnO) is only present in detectable amounts in the rinds (0.2%). Pockets of MnO are located in interior edges of the rinds along more permeable laminae and are also visible in BSE images (Fig. 6A,B).

Porosity in the solid sample analyzed with QEMSCAN is 4%. HFO cement is 24% of total composition (including framework grains and porosity). Kaolinite is present in minor amounts (0.7%).

Two textures of HFO cement are identified with QEMSCAN. The most abundant type is a smooth textured HFO visible in back scattered electron (BSE) images and labeled "HFO" in the figures (Fig. 6C,D). The other is a "frothy" textured cement in BSE images and is labeled "HFO Textures" in the figures (Fig. 6C,D). Smooth-textured HFO is the most abundant phase in the rinds (94.5%), but in the interiors, the HFO cement is distributed evenly between smooth-textured (20.0%) and frothy-textured (26.8%).

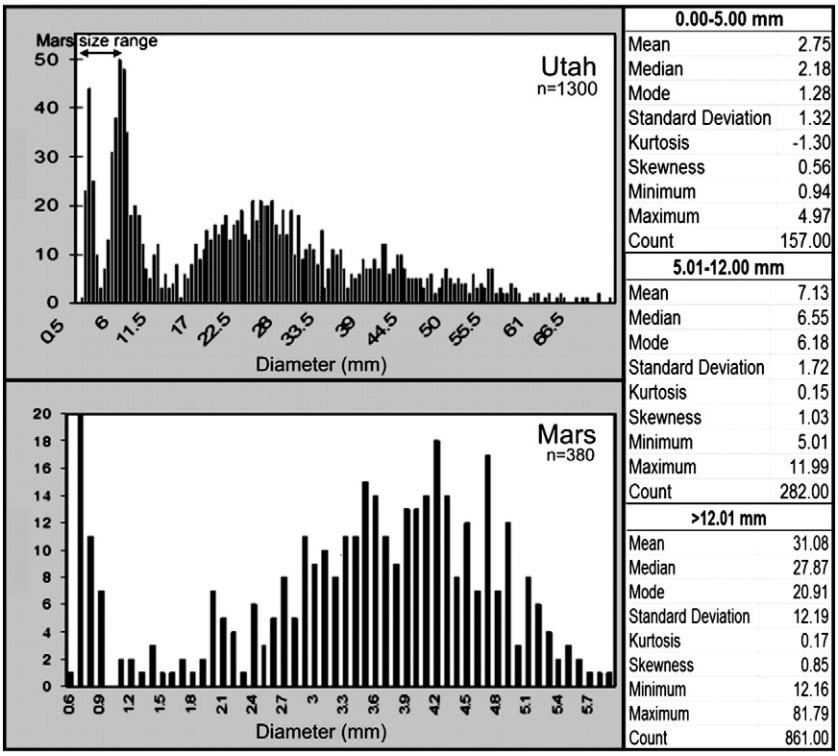

0.00-5.00 mm	
Mean	2.75
Median	2.18
Mode	1.28
Standard Deviation	1.32
Kurtosis	-1.30
Skewness	0.56
Minimum	0.94
Maximum	4.97
Count	157.00
5.01-12.00 mm	
Mean	7.13
Median	6.55
Mode	6.18
Standard Deviation	1.72
Kurtosis	0.15
Skewness	1.03
Minimum	5.01
Maximum	11.99
Count	282.00
>12.01 mm	
Mean	31.08
Median	27.87
Mode	20.91
Standard Deviation	12.19
Kurtosis	0.17
Skewness	0.85
Minimum	12.16
Maximum	81.79
Count	861.00

Fig. 4. Comparison of Utah and Mars concretion diameter data. Descriptive statistics are for Utah size ranges <5 mm, 5–12 mm and >12 mm. Mars data is from Calvin et al. (2008). Note Mars size range compared to Utah (top left on Utah graph).

4.3. VNIR reflectance spectroscopy

Characteristic absorption features for minerals in this study are: hematite (~871 nm), goethite (~894 nm), lepidocrocite (~933 nm), ferrihydrite (~949 nm), kaolinite (~2200 nm) and illite (~2200 nm). Kaolinite is distinguished from illite by shoulders at ~2180 nm and 1490 nm. There are also OH^- absorption features at ~1400 nm and ~1900 nm associated with ferrihydrite, lepidocrocite, kaolinite and illite; however, the clay absorption features can interfere with the OH^- features of the HFOs when both clays and HFOs are present (Clark, 1999; Clark et al., 1990).

Three phases of HFO are detected using VNIR reflectance spectroscopy in the macro-concretions. Goethite and hematite are straightforward to interpret in these samples. A third phase has an absorption minima that fall typically >940 nm, suggesting that it is ferrihydrite. However, this phase also has a shoulder at ~670 nm, which is indicative of lepidocrocite. Lepidocrocite has an absorption minimum around 930 nm, which is lower than the phase detected. Pending further study, this phase is herein referred to as amorphous HFO and is discussed in depth in Section 6.

Transects across rind macro-concretions (n = 10) always reveal amorphous HFO in at least one side of the rind (Fig. 7A). The opposite rind cements are either amorphous HFO or goethite except for two samples that showed absorption minima in the hematite range. The HFO phases in the interiors exhibit absorption minima in the hematite, goethite or a mixture of hematite and goethite ranges. Kaolinite is detected in all the interior spectra and one of the rind spectra; probable minor illite is detected in one of the interior spectra.

For layered concretions (n = 5), the absorption minima for HFO cements are predominately in the goethite range; one sample had an absorption minimum in the amorphous HFO range (Fig. 7B). Hematite cement is detected in the depleted interior of one layered concretion sample.

Results from two solid samples show absorption minima in the amorphous HFO and goethite ranges (Fig. 7C). Neither sample contains any detectable hematite.

5. Analytical interpretation

The presence of three generations of isopachous cements implies that the concretions grew via a pervasive growth model where HFO nucleated at sites concurrently throughout the concretion similar to some carbonate concretions. HFO gel likely precipitated and sets the radius with some retained porosity (see Raiswell et al., 2000 for a discussion on pervasive growth in carbonate concretions). Therefore, original porosity of the rinds was much higher than present porosity (2%). Reactants could diffuse through the higher porosity rinds precipitating additional isopachous cements that filled retained, original porosity and modified internal structures. Macroscopic and microscopic inward digitate cements provide additional evidence for the inward growth model.

With QEMSCAN, two textural HFO phases are detected and are present in predictable places. Manganese oxide pockets also occur as a late-stage, pore filling typically along interior edges of rinds and along more permeable laminae. The manganese oxide precipitate could be due to a rise in pH in the mineralizing fluid; manganese oxide precipitates at a slightly higher pH (~7.8) than HFO (~5.8) (Stumm and Morgan, 1996).

The amorphous HFO phase detected with VNIR reflectance spectroscopy is problematic. The absorption feature at >940 nm would indicate that it is possibly ferrihydrite. Ferrihydrite is a nanophase $Fe(OH)_3$ that ranges from amorphous to partly crystalline (Carlson and Schwertmann, 1981; Cornell and Schwertmann, 1996). Ferrihydrite has similar Mössbauer parameters to the nanophase Fe^{3+} oxide detected in the concretions (IS = 0.35 and QS = 0.83–0.90 or 0.53 mm/s; see Supplemental section for Mössbauer spectroscopy

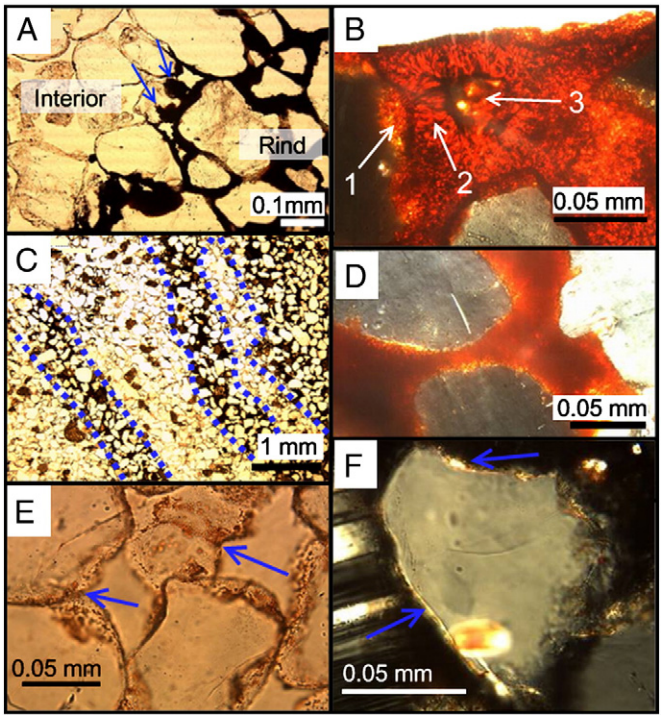

Fig. 5. Photomicrographs of macro-concretions. A. Rind/interior boundary of a rind concretion (plane light). Blue arrows point to digitate inward growths of HFO cement. B. Three phases of HFO cement (polarized light): 1. granular cement rimming edges of quartz grains, 2. tabular cement, and 3. small, euhedral crystals infilling remaining pore space. C. Layered concretion (plane light). Blue dotted lines delineate well-cemented layers from more friable areas. D. Granular HFO cement in solid concretion (polarized light). E. Interior of rind concretion (plane light). Arrows point to granular HFO cement in pore throats and rimming quartz grains. F. Quartz grain with high birefringence illite rim (arrows) in rind concretion interior (polarized light).

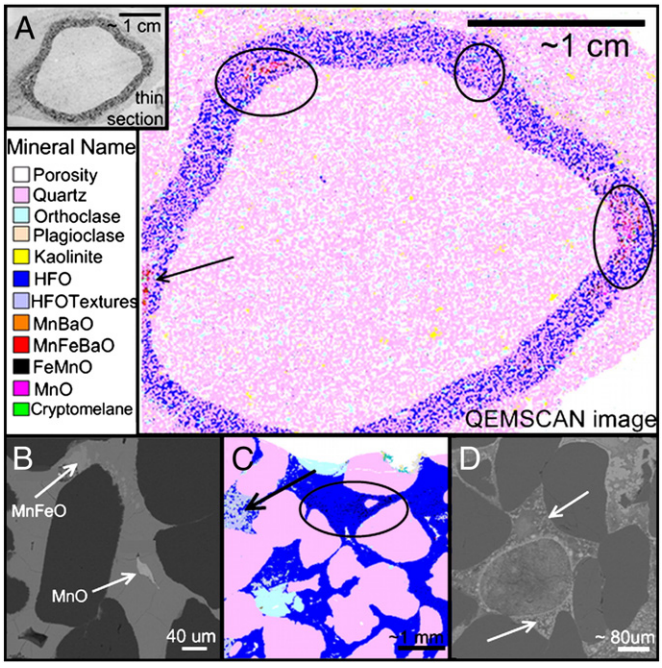

Fig. 6. QEMSCAN images (A, C) and back scattered electron (BSE) images (B, D) A. Discoidal rind concretion. Inset is photograph of thin section used to acquire QEMSCAN image. Arrow and circles point to pockets of MnO. These pockets occur along more permeable eolian grainflow laminae of the host rock. B. Rind area. Arrows point to late-stage MnO pore filling shown in light gray. Dark gray is the more abundant, smooth textural phase of HFO labeled "HFO" in key. Black areas are quartz grains. C. Rind area at 1 μm pixel spacing. Black oval encircles area with concentration of FeMnO in HFO cement. Arrow points to frothy HFO. D. "Frothy" textured cement (arrows) in rind.

results). Ferrihydrite is a very unstable HFO phase and at intermediate pH and diagenetic temperatures (~70 °C), it recrystallizes to more stable phases in a matter of weeks in laboratory experiments (Cornell and Schwertmann, 1996; Kukkadapu, 2003). However, some research suggests that coprecipitation with nickel inhibits the recrystallization of ferrihydrite into more stable phases (Kukkadapu, 2003) and the Navajo Sandstone concretions are enriched in nickel relative to the host rock (Potter and Chan, submitted for publication).

Another possibility is that this phase at >940 nm is lepidocrocite. Lepidocrocite is a metastable γ-FeOOH. Lepidocrocite has a distinct shoulder at ~670 nm and an absorption minimum of ~930 nm. The shoulder feature is present in the amorphous HFO phase in the concretions, but many of the absorption minima are >940 nm.

HFO can precipitate as an amorphous gel that dehydrates to goethite and then hematite with heat or age (Klein and Bricker, 1977). The Navajo Sandstone represents a low temperature diagenetic system (<100 °C; Parry et al., 2004); therefore, the amorphous HFO is a younger phase because the minerals are dehydrating via time rather than heat. Similarly, the goethite is interpreted to be intermediate in age and the hematite is likely the oldest phase.

A late stage precipitation event is documented in the study area (~5 Ma Potter and Chan, submitted for publication), so a very young, unstable HFO phase could be overprinted on the concretions. This young HFO (identified herein as amorphous HFO) could be amorphous, nanophase ferrihydrite (stabilized by coprecipitation with nickel) or ferrihydrite that later partially recrystallized while still retaining the ferrihydrite range (>940 nm) absorption minimum (Bishop et al., 2006). The presence of the three HFO phases implies that the HFO was precipitated as an amorphous ferrihydrite and has dehydrated to more stable phases with time instead of precipitating directly as hematite or goethite. Further work is necessary to precisely determine the composition of the amorphous HFO phase.

Layered and solid concretions exhibit younger HFO phases (amorphous HFO and goethite) throughout the interiors relative to the older phase (hematite) in the interiors of rind concretions. Higher initial porosity rinds (evidenced by isopachous cements) may have allowed reactants to diffuse through, creating the layered and solid end-members. The presence of Liesegang bands in the interiors of both rind and layered macro-concretions supports the premise that these concretions initially precipitated as rind concretions and internal structures were modified by subsequent inward diffusive mass transfer.

Mössbauer data (see Supplemental section) show multiple overlapping peaks that are difficult to fit uniquely; however, the results generally show at least three phases of HFO: a nanophase (or amorphous) HFO, goethite and hematite. These are consistent with the three phases detected with VNIR reflectance spectroscopy (amorphous HFO, goethite and hematite). Because the samples analyzed with Mössbauer spectroscopy are from a broad area over southern Utah, this suggests that multiple precipitation events have affected the Navajo Sandstone regionally.

6. Discussion

The range of physical characteristics, internal structures and cement phases (textural, mineralogical and chemical) all suggest a complex diagenetic history of repeated iron mobilization and precipitation events for the Navajo Sandstone. The major implications of this research are the complexities of the concretion formation model proposed herein, and the establishment of diagnostic criteria for distinguishing diagenetic concretion formation.

A synthesis of the results suggests that multiple precipitation events overprinted original HFO concretions with additional cements

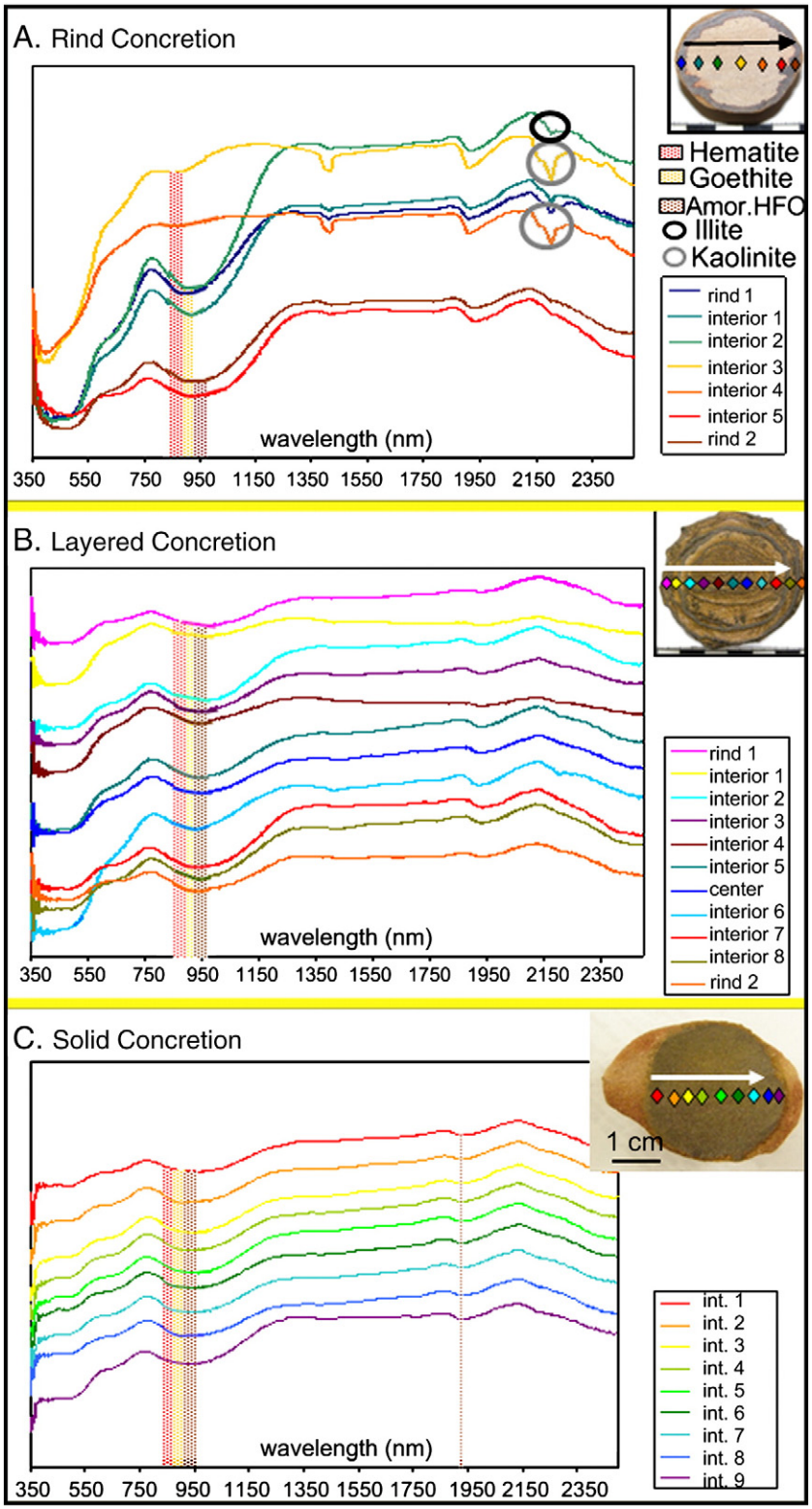

Fig. 7. Typical VNIR spectra in transects across rind, layered and solid end members. Y-axis represents reflectance. A. Rind concretion. Transect across the center of the concretion is shown in photo. Rind 1 is goethite; Rind 2 is amorphous HFO; interiors 3 and 4 are hematite. Kaolinite peaks are circled with gray; probable illite peak is circled with black. B. Layered concretion. HFO phases throughout the transect are amorphous HFO. Interior 6 shows probable minor illite, but most of the readings show no clays probably due to interference with the HFO. C. Solid concretion spectra showing amorphous HFO across transect. Sample includes some host rock, but spectra are only shown for concretion.

(HFO and MnO) throughout the diagenetic history of the Navajo Sandstone in Spencer Flat. Concretions were altered both mineralogically and structurally by generations of fluids with varying chemistries throughout diagenesis. Younger cement phases were added by late stage precipitation as reactants diffused through higher initial porosity rinds to structurally alter interiors. Even in disparate sample locations (~100 km apart), multiple fluids and precipitation events influenced the mineralogy of concretions. In some cases, concretions provided nuclei around which smaller micro-concretions coalesce introducing a component of radial growth.

Table 2
Similarities between the Burns formation spherules and proposed terrestrial analogs. Entries based on characterization of Martian blueberries and comparison to terrestrial analogs by Calvin et al. (2008), but including data from this study.

Analogs and models	Mars[a]	Utah[b] (ancient) (this study)	Acid saline lake concretions[c] (modern)	Mauna Kea spherules[d]	Impact lapilli[e]
Host rock characteristics					
Fine-grained, homogenous, eolian sedimentary host rock	X	X			
Host rock spans >100,000 km^2 area	X	X			X
Host rock composition	Sulfate, basaltic	Quartz arenite	Evaporites	Basalt	Greenstone belt
Concretion physical characteristics					
Spheroidal geometry	X	X	X	X	X
Latitudinal ridges or furrows	Rare	Present	?		
Doublets or triplets	Present	Present	?	Present	Present
Locally abundant doublets	X	X	?		
Adhered host rock	Present	Present	?		
Interior structure	Solid	Rind, layered, solid	Solid	Solid, rind?	Solid
Polymodal distribution	X	X	?	?	
<1 mm dia	X			X	
1–2 mm to 5 mm dia	X	X			X
>5 mm dia		X	X		
Two size ranges in single horizon	Common	Common	?		
Self-organized spacing	X	X	?		
Vertically distributed through 10s of meters of section	X	X	?		
3D distribution throughout host rock	X	X	?		
% volume	3.2	1.2	~1.8		
Concretion mineralogical characteristics					
Cement mineralogy					
Hematite	X	X	X	X	Glass precursor
Goethite	Precursor	X	Rare		
Jarosite	X		X		
Nanophase HFO	X	X	?		
Clays	?	X	X		
Clastic grain component	?	Quartz	Gypsum, quartz		
Enriched in Ni relative to host rock	X	X			X
Radial crystal growth	X			X	

[a] Calvin et al. (2008).
[b] This study.
[c] Benison (2006), Benison and Bowen (2006), Benison et al. (2007), and Bowen et al. (2008).
[d] Morris et al. (2005).
[e] Knauth et al. (2005).

In isotopic studies of Navajo Sandstone concretions in Spencer Flat, Busigny and Dauphas (2007) showed an increasingly negative isotopic signature in an easterly direction and concluded that concretions precipitated in one precipitation event that swept through Spencer Flat. Iron isotope studies by Chan et al. (2006) showed zonation across individual concretions from multiple localities, but no directional isotopic trends across the region. Interestingly, isotopic zonation across concretions from the rinds to the interiors is increasingly lighter in some concretions and increasingly heavier in others. The conclusions of these isotope studies seemingly contradict the model of pervasive concretion growth affected by multiple precipitation events proposed herein; however, the zonation in concretions could be due to the subsequent precipitation of cements by fluids with varying isotopic signatures. The Busigny and Dauphas (2007) interpretation of concretion precipitation in one event is easily reconciled with our pervasive growth model where an initial event precipitates most of the iron in the concretion and sets the radius. There is some retained porosity in the concretions that is later infilled by subsequent, smaller amounts of cements that do not affect the overall bulk isotopic signatures of the concretions significantly. Furthermore, varying amounts of secondary concretion cements with different isotopic compositions may well explain the variability in the bulk isotopic signatures (illustrated in Fig. 7 of Busigny and Dauphas, 2007). Potter and Chan (submitted for publication) show that multiple precipitation events have affected the Spencer Flat area throughout geologic time deduced from cross-cutting field relationships of HFO precipitation geometries. The research presented herein examined cements on a micron scale and the evidence for multiple precipitation events exists in isopachous cements in pore spaces. Both Busigny and Dauphas (2007) and Chan et al. (2006) sampled cements on a millimeter scale and these samples could contain cements from more than one event, which would effectively smear the isotopic signature. The ambiguities between the isotope investigations and this field and laboratory research show the need for higher resolution techniques for *in situ* iron isotope studies in diagenetic cements.

HFO can result from the oxidation of reduced iron mineral phases such as pyrite or siderite; however, four lines of evidence support the interpretation of direct precipitation of primary HFO cement: 1. Multiple phases of HFO (including an amorphous phase) suggest that the iron precipitated as an amorphous HFO that has oxidized to more stable phases over geologic time. 2. The lack of crystal pseudomorphs (only two HFO after pyrite pseudomorphs were observed in 90 thin sections). 3. The lack of any pyrite or siderite in the concretion cements. 4. The lack of Fe^{2+} valance state in the concretions (see Supplemental section for Mössbauer spectroscopy results). The possibility that all of the siderites have been oxidized is unlikely because carbonate interdune deposits (calcite and siderite) are still present throughout the Navajo Sandstone (Parrish and Falcon-Lang, 2007) as well as in the Spencer Flat study area. Sulfur is also not detected in the concretions or the host rock with whole rock analysis; it is likely that traces would remain if the concretions were originally pyrite (Beitler, 2005; Potter and Chan, submitted for publication).

Complex mass transfer processes and fluid chemistries affect water/rock interactions throughout the diagenetic history of a sandstone. HFO concretions preserve important information about the diagenetic evolution of a sandstone reservoir. This characterization provides an

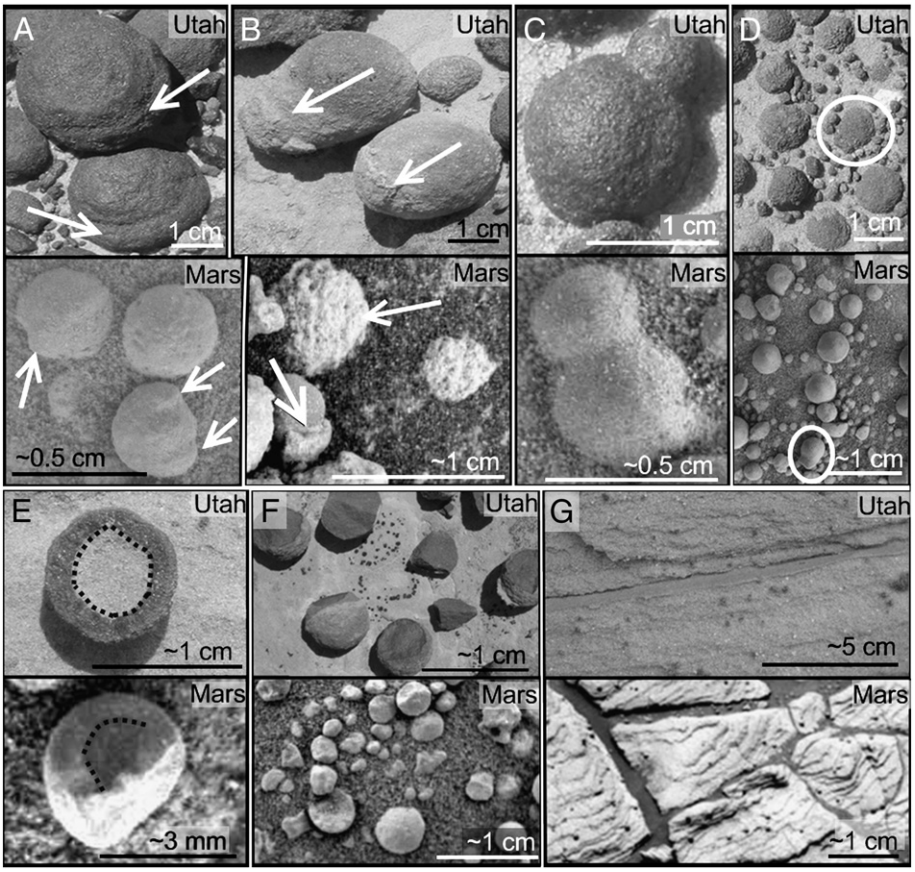

Fig. 8. Host rock and exterior structural similarities between Utah (top images for each set) and Mars (bottom images). A. Ridges and furrows (arrows) B. Weathered out spherules with asymmetrical adhered host rock (bottom arrow in Mars image). Top arrow in Mars image points to "avocado skin" exterior texture. See Figure 2E for similar "avocado skin" Utah example. C. Doublets. D. Two size populations of weathered out concretions and a "duckbill" shape (circles). E. Rind or concentric zonation (dotted lines). F. Solid internal structure. G. *In situ* concretions showing self-organized spacing. Mars images: NASA/JPL/Cornell.

excellent analog model to illuminate diagenetic processes in other settings including the Burns formation hematite spherules in Meridiani Planum, Mars. The concretion features documented comprise diagnostic criteria for diagenetic concretion formation and are compared with a similar characterization on the Burns formation spherules by Calvin et al. (2008) as well as to other proposed analog models from the literature (Table 2).

7. Utah and Mars comparison

The Navajo Sandstone and the Burns formation are both fine-grained, eolian sandstones with an areal extent >100 km^2 (Grotzinger, 2005). Both units are porous and permeable media in which there is evidence of groundwater diagenesis (McLennan, 2005). The main difference between the two units is geochemical: the Burns formation is composed of soluble sulfate sands and the Navajo Sandstone is a clean quartz arenite (Grotzinger, 2005; Squyres, 2004). Concretions, however, are known to form in a variety of host rock compositions and exhibit a broad range of mineralogies. Physical formation mechanisms are independent of host rock composition; host rock composition affects chemical and mineralogical characteristics such as crystallinity, chemical composition, and sphericity. Because of the major differences in geochemical composition of the host rock, physical characteristics are discussed separately from the mineralogical and crystallographic comparison in the following comparison.

7.1. Physical characteristics

The Utah concretions range from spheroidal (aspect ratio ranges from 1.00 to 1.06) to discoidal (aspect ratio = 1.06–2.00) and have a mean aspect ratio of 1.10 (Potter and Chan, submitted for publication). Mars spherules have a similar range with a mean aspect ratio of 1.06 (McLennan, 2005). Surficial, latitudinal ridges or furrows around the perimeter of the spherules are present in both Utah and Mars examples (Fig. 8A), although these are much more common in Utah than on Mars. These ridges align with laminae when concretions are *in situ* in both Utah and Mars and result from cementation in a sedimentary rock. The likely reason these ridges are more common in Utah than on Mars is because of stronger anisotropies in the Navajo Sandstone bedding.

There are samples from both Utah and Mars that exhibit an "avocado skin" texture (Figs. 1E [Utah] and 8B [Mars, Calvin et al., 2008]). In Utah, this texture is the result of multiple nucleation sites precipitating clusters of micro-concretions that coalesce to form the larger concretions in an Ostwald ripening process. A similar nucleation phenomenon could be responsible for bumpy-textured concretion formation on Mars where smaller spherules dissolve and reprecipitate on larger spherules (Calvin et al., 2008) or this texture could result from secondary cements (McLennan, 2005).

Occasional doublets, triplets and "duckbill" shapes occur in both Utah concretions and Mars spherules (Fig. 8C,D; Calvin et al., 2008). In Meridiani Planum, an abundant population of doublets is present near a large impact crater (Calvin et al., 2008). An abundant localized population of doublets also is present in the Spencer Flat area, suggesting a restricted nucleation process responsible for the doublet morphology.

Some well-cemented Utah and Mars samples weather out with preferentially cemented host rock adhered to the exterior (Fig. 8B; Calvin et al., 2008). In Utah, this preferential cementation surrounding *in situ* concretions results from late stage precipitation events that

preferentially cement host rock grains in an asymmetric "comet tail" shape in the direction of fluid flow (Potter and Chan, submitted for publication). The presence of similarly cemented asymmetric forms on Mars suggests that although the diagenetic history is simpler, more than one precipitation event likely occurred. Spheroidal concretions precipitated via diffusive mass transfer; asymmetrical "comet tails" precipitate by advective mass transfer (McBride et al., 2003, 1994; Mozley and Davis, 2005; Mozley and Goodwin, 1995; Potter and Chan, submitted for publication).

Internal structure of the Utah macro-concretions comprises three end-members: rind, layered, and solid (Fig. 1A,B,C). Utah micro-concretions have two end-members: rind and solid, although most micro-concretions exhibit solid interiors (Calvin et al., 2008). The Mars spherules typically exhibit solid internal structure; however, possible rind internal structures are documented on Mars (Fig. 8E,F; Calvin et al., 2008). The higher variety of internal structures implies that the Navajo Sandstone experienced a much more complex diagenetic history than the Burns formation.

Mars size populations have similar divisions of micro- and macro- to the Utah concretions; however, on Mars, micro-spherules are <1 mm diameter and macro-spherules are typically 1–6 mm diameter (Fig. 4; Calvin et al., 2008). Calvin et al. (2008) suggest that the geochemistry in the Burns formation is water-limited. Water-limited geochemical conditions could result in smaller spherules, in contrast to the long history of abundant water in the Navajo Sandstone. The size difference between Utah concretions and Mars spherules suggests that although groundwater was present on Mars at some point, it may have been more scarce and ephemeral relative to Earth.

Utah and Mars examples exhibit more than one size range present together in outcrop and both examples exhibit *in situ* geochemically self organized spacing (Fig. 8G; Calvin et al., 2008; McLennan, 2005). Volumetric density for Utah concretions is 1.2% (Potter and Chan, submitted for publication) and 3.2% for Mars spherules (McLennan, 2005). Spatial distribution in both Utah and Mars extends over a km-scale area and through 10s of meters of vertical section (Calvin et al., 2008; Squyres, 2009). Both Mars and Utah exhibit polymodal size distributions (Fig. 4).

7.2. Mineralogy and crystallography

The HFO cement mineralogy is more intricate in Utah concretions than in Mars spherules, although some important similarities exist. Three phases of HFO cement (amorphous HFO, goethite, and hematite) are present in the Utah concretions, which likely precipitated as amorphous HFO gel and dehydrated with age to more stable goethite and hematite. The shape of the Mini-TES spectra indicates that the Martian spherules likely precipitated as an oxyhydroxide precursor mineral phase (such as a precursor gel phase) that later dehydrated to hematite (Glotch et al., 2004). Both the Utah concretions and the Mars spherules are enriched in Ni relative to the host rock (Morris et al., 2006). The Mössbauer spectroscopy results suggest that the Navajo Sandstone concretions are hematite or goethite with a nanophase Fe^{3+} oxide; a similar nanophase Fe^{3+} oxide signature is present in the Burns formation (Klingelhoefer et al., 2004; Morris et al., 2006).

One crystallographic difference between the Mars and the Utah examples is that the Mars spherules have radial crystal structure and high crystallinity (Calvin et al., 2008). The sulfate sandstone of the Burns formation is composed of reactive, soluble grains that partially dissolved—leaving voids in the host rock—during or prior to the precipitation of the spherules. These voids allow more space for higher sphericity geometry and euhedral crystal growth preferentially oriented along the c-axis. The Navajo Sandstone is a quartz arenite formed from relatively insoluble grains so the HFO precipitate would not have the same room to form euhedral crystals as in Mars spherules.

The Burns formation contains silicate minerals derived from aqueous alteration of olivine basalt mixed with sulfate minerals, including jarosite. Jarosite is still present in outcrops, which indicates that, in Meridiani Planum, diagenetic fluids were pH<4–5 (Madden et al., 2004; Tosca et al., 2005). The Navajo Sandstone concretions were likely precipitated at circumneutral pH (Beitler, 2003, 2005; Busigny and Dauphas, 2007; Chan et al., 2000, 2004, 2005, 2007).

The Mars spherules may also exhibit a higher degree of crystallinity due to greater iron abundance in the Burns formation sediments. The Burns formation spherules may have formed via the dissolution of iron-bearing sulfates (such as jarosite) during diagenesis (McLennan, 2005; Tosca et al., 2005). The Navajo Sandstone iron was sourced from the breakdown of ferromagnesian minerals during deposition and early burial of the erg (Chan et al., 2000, 2004, 2007). This more euhedral crystal structure on Mars would also account for color differences between Mars and Utah spherules because hematite crystals appear grey when they are larger than 5 μm and reddish brown when they are smaller than 5 μm.

Other proposed non-concretion analog models (e.g., impact lapilli, Knauth et al., 2005; Mauna Kea spherules, Golden et al., 2008; Morris et al., 2005) can generate spheroidal geometry but lack other key physical characteristics (Table 2). However, other analog models may provide better geochemical information due to formation in acidic sulfate-rich environments (e.g., Mauna Kea, Golden et al., 2008; Morris et al., 2005 and acid saline lakes, Bowen et al., 2008). Although no perfect terrestrial analog exists for the Mars spherules, the Navajo Sandstone concretions share diagnostic physical similarities to important characteristics of the Burns formation spherules and thus, it is clear that diagenetic groundwater and diffusive mass transfer are responsible for the formation of the Mars spherules.

Supplementary materials related to this article can be found online at doi:10.1016/j.epsl.2010.11.027.

Acknowledgements

This research was funded by NASA Mars Fundamental Research (NNG06GI10G), a BLM Grand Staircase-Escalante National Monument grant (both to Chan) and an Exxon-Mobil Student Research grant (to Potter). An NSF grant (0811250) provided funding for Potter to participate in an ADVANCE-Nebraska writing workshop. We gratefully acknowledge Lori Kormos for help with QEMSCAN and Mary Anne Holmes and John Bowman for the help in editing the manuscript. We thank Vincent Busigny and an anonymous reviewer for insightful feedback that strengthened this manuscript.

References

Barge, L.M., Petruska, J., 2007. Iron precipitation patterns in gels; implications for the formation of hematite concretions at Meridiani Planum, Mars. Abstracts of Papers Submitted to the Lunar and Planetary Science Conference, 38.

Beitler, B., 2003. Bleaching of Jurassic Navajo Sandstone on Colorado Plateau Laramide highs; evidence of exhumed hydrocarbon supergiants? Geology 31, 1041–1044.

Beitler, B., 2005. Fingerprints of fluid flow; chemical diagenetic history of the Jurassic Navajo Sandstone, southern Utah, U.S.A. J. Sed. Res. 75, 547–561.

Benison, K., 2006. A Martian analog in Kansas; comparing Martian strata with Permian acid saline lake deposits. Geology 34, 385–388.

Benison, K., Bowen, B., 2006. Acid saline lake systems give clues about past environments and the search for life on Mars. Icarus 183, 225–229.

Benison, K., Bowen, B.B., Oboh–Ikuenobe, F.E., Jagniecki, E.A., LaClair, D.A., Story, S.L., Mormile, M.R., Hong, B., 2007. Sedimentology of acid saline lakes in southern Western Australia; newly described processes and products of an extreme environment. J. Sed. Res. 77, 366–388.

Bishop, J.L., Dyar, M.D., Parente, M., Drief, A., Mancinelli, R.L., Lane, M.D., Murad, E., 2006. Anonymous, Understanding surface processes on Mars through study of iron oxides/oxyhydroxides; clues to surface alteration and aqueous processes. Abstracts of Papers Submitted to the Lunar and Planetary Science Conference, 37.

Blakey, R., 1994. Paleogeographic and tectonic controls on some Lower and Middle Jurassic erg deposits. Colorado Plateau Mesozoic systems of the Rocky Mountain region, USA. 273 pp.

Blakey, R., Peterson, F., Kocurek, G., 1988. Syntheses of late Paleozoic and Mesozoic eolian deposits of the Western Interior of the United States. Sed. Geol. 56, 3–125.

Boles, J.R., Landis, C.A., Dale, P., 1985. The Moeraki Boulders; anatomy of some septarian concretions. J. Sed. Petrol. 55, 398–406.
Bowen, B., Martini, B.A., Chan, M.A., Parry, W.T., 2007. Reflectance spectroscopic mapping of diagenetic heterogeneities and fluid-flow pathways in the Jurassic Navajo Sandstone. AAPG Bull. 91, 173–190.
Bowen, B., Benison, K.C., Oboh-Ikuenobe, F.E., Story, S., Mormile, M.R., 2008. Active hematite concretion formation in modern acid saline lake sediments, Lake Brown, Western Australia. Earth Planet. Sci. Lett. 268, 52–63.
Busigny, V., Dauphas, N., 2007. Tracing paleofluid circulations using iron isotopes; a study of hematite and goethite concretions from the Navajo Sandstone (Utah, USA). Earth Planet. Sci. Lett. 254, 272–287.
Calvin, W.M., Shoffner, J.D., Johnson, J.R., Knoll, A.H., Pocock, J.M., Squyres, S.W., Weitz, C.M., Arvidson, R.E., Bell III, J.F., Christensen, P.R., de Souza Jr., P.A., Farrand, W.H., Glotch, T.D., Herkenhoff, K.E., Jolliff, B.L., Knudson, A.T., McLennan, S.M., Rogers, A. D., Thompson, S.D., 2008. Hematite spherules at Meridiani; results from MI, Mini-TES, and Pancam. J. Geophys. Res. 113.
Carlson, L., Schwertmann, U., 1981. Natural ferrihydrites in surface deposits from Finland and their association with silica. Geochim. Cosmochim. Acta 45, 421–429.
Chan, M., Parry, W.T., Bowman, J.R., 2000. Diagenetic hematite and manganese oxides and fault-related fluid flow in Jurassic sandstones, southeastern Utah. AAPG Bull. 84, 1281–1310.
Chan, M., Parry, W., Beitler, B., Ormö, J., Komatsu, G., 2004. A possible terrestrial analogue for haematite concretions on Mars. Nature 429, 731–734.
Chan, M., Bowen, B., Parry, W., Ormö, J., Komatsu, G., 2005. Red rock and red planet diagenesis; comparisons of Earth and Mars concretions. GSA today 15, 4–10.
Chan, M.A., Johnson, C.M., Beard, B.L., Bowman, J.R., Parry, W.T., 2006. Iron isotopes constrain the pathways and formation mechanisms of terrestrial oxide concretions; a tool for tracing iron cycling on Mars? Geosphere 2, 324–332.
Chan, M.A., Ormoe, J., Park, A.J., Stich, M., Souza-Egipsy, V., Komatsu, G., 2007. Models of iron oxide concretion formation; field, numerical, and laboratory comparison. Geofluids 7, 356–368.
Clifton, H., 1957. The carbonate concretions of the Ohio Shale. Ohio J. Sci. 57, 114–124.
Coleman, M.L., Raiswell, R., 1981. Carbon, oxygen and sulphur isotope variations in concretions from the upper Lias of N.E. England. Geochim. Cosmochim. Acta 45, 329–340.
Coleman, M., Raiswell, R., 1995. Source of carbonate and origin of zonation in pyritiferous carbonate concretions; evaluation of a dynamic model. Am. J. Sci. 295, 282–308.
Clark, R., 1999. Spectroscopy of rocks and minerals and principles of spectroscopy, 3rd Edition. Remote Sensing for the Earth Sciences—Manual of Remote Sensing, Volume 3, pp. 3–58.
Clark, R.N., King, T.V.V., Klejwa, M., Swayze, G.A., Vergo, N., 1990. High spectral resolution reflectance spectroscopy of minerals. J. Geophys. Res. 95, 12653–12680.
Clark, R.N., Swayze, G.A., Wise, R.A., Livo, K.E., Hoefen, T.M., Kokaly, R.F., Sutley, S.J., 2007. USGS Digital Spectral Library splib06a, U. S. Geological Survey Data Series, Report: DS0231.
R.M. Cornell, U. Schwertmann, The iron oxides; structure, properties, reactions, occurrence and uses, VCH Verlagsgesellschaft, Weinheim, Federal Republic of Germany (DEU) 1996, p. 573.
Dickson, J.A.D., Barber, C., 1976. Petrography, chemistry and origin of early diagenetic concretions in the lower Carboniferous of the Isle of Man. Sedimentology 23, 189–211.
Eichhubl, P., Taylor, W.L., Pollard, D.D., Aydin, A., 2004. Paleo-fluid flow and deformation in the Aztec Sandstone at the Valley of Fire, Nevada; evidence for the coupling of hydrogeologic, diagenetic, and tectonic processes. Geol. Soc. Am. Bull. 116, 1120–1136.
Feistner, K.W.A., 1989. Petrographic examination and re-interpretation of concretionary carbonate horizons from the Kimmeridge Clay, Dorset. J. Geol. Soc. 146, 345–350.
Glotch, T.D., Morris, R.V., Christensen, P.R., Sharp, T.G., 2004. Effect of precursor mineralogy on the thermal infrared emission spectra of hematite; application to Martian hematite mineralization. J. Geophys. Res. 109.
Golden, D.C., Ming, D.W., Morris, R.V., Graff, T.G., 2008. Hydrothermal synthesis of hematite spherules and jarosite: implications for diagenesis and hematite spherule formation in sulfate outcrops at Meridiani Planum, Mars. Am. Mineralog. 93, 1201–1214.
Grotzinger, J., 2005. Stratigraphy and sedimentology of a dry to wet eolian depositional system, Burns Formation, Meridiani Planum, Mars. Earth Planet. Sci. Lett. 240, 11–72.
Hudson, J.D., 1978. Concretions, isotopes, and the diagenetic history of the Oxford Clay (Jurassic) of central England. Sedimentology 25, 339–367.
Huggett, J.M., 1994. Diagenesis of mudrocks and concretions from the London Clay Formation in the London Basin. Clay Miner. 29, 693–707.
Jordan, M.M., Aplin, A.C., Curtis, C.D., Coleman, M.L., 1992. Access of pore waters to carbonate precipitation sites during concretion growth. Proc. Int. Symp. Water Rock Interact. 7, 1239–1242.
Klein, C., Bricker, O.P., 1977. Some aspects of the sedimentary and diagenetic environment of Proterozoic banded iron-formation. Econ. Geol. Bull. Soc. Econ. Geol. 72, 1457–1470.
Klingelhoefer, G., Morris, R.V., Bernhardt, B., Schroeder, C., Rodionov, D.S., de Souza, P.A., Yen, A., Gellert, R., Evlanov, E.N., Zubkov, B., Foh, J., Bonnes, U., Kankeleit, E., Guetlich, P., Ming, D.W., Renz, F., Wdowiak, T., Squyres, S.W., Arvidson, R.E., Rowan, L., 2004. Jarosite and hematite at Meridiani Planum from Opportunity's Mössbauer spectrometer. Science 306, 1740–1745.
Knauth, L.P., Burt, D.M., Wohletz, K.H., 2005. Impact origin of sediments at the Opportunity landing site on Mars. Nature 438, 1123–1128.
Kukkadapu, R.K., 2003. Transformation of 2-line ferrihydrite to 6-line ferrihydrite under oxic and anoxic conditions. Am. Mineralog. 88, 11–12.
Lane, M., Morris, R.V., Christensen, P.R., 1999. The spectral behavior of hematite at visible/near infrared and midinfrared wavelengths; application to Mars. Abstr. Programs Geol. Soc. Am. 31, 46.
Lyons, T., Raiswell, R., Robinson, A., Scott, C., Chu, X., Li, C., Love, G., Sessions, A., Gill, B., 2007. Carbonate concretions as a window to the evolving chemistry of the early ocean and atmosphere. Geochim. Cosmochim. Acta 71, A606.
Madden, M.E.E., Bodnar, R.J., Rimstidt, J.D., 2004. Jarosite as an indicator of water-limited chemical weathering on Mars. Nature 431, 821–823.
McBride, E.F., Picard, M.D., Folk, R.L., 1994. Oriented concretions, Ionian Coast, Italy; evidence of groundwater flow direction. J. Sed. Res. A Sed. Petrol. Process. 64, 535–540.
McBride, E., Picard, M.D., Milliken, K.L., 2003. Calcite-cemented concretions in Cretaceous sandstone, Wyoming and Utah, U.S.A. J. Sed. Res. 73, 462–484.
McLennan, S., 2005. Provenance and diagenesis of the evaporite-bearing Burns Formation, Meridiani Planum, Mars. Earth Planet. Sci. Lett. 240, 95–121.
Morris, R., Ming, D.W., Graff, T.G., Arvidson, R.E., Bell, J.F., Squyres, S.W., Mertzman, S.A., Gruener, J.E., Golden, D.C., Le, L., Robinson, G.A., 2005. Hematite spherules in basaltic tephra altered under aqueous, acid-sulfate conditions on Mauna Kea volcano, Hawaii; possible clues for the occurrence of hematite-rich spherules in the Burns Formation at Meridiani Planum, Mars. Earth Planet. Sci. Lett. 240, 168–178.
Morris, R.V., Klingelhoefer, G., Schroeder, C., Rodionov, D.S., Yen, A., Ming, D.W., de Souza Jr., P.A., Wdowiak, T., Fleischer, I., Gellert, R., Bernhardt, B., Bonnes, U., Cohen, B.A., Evlanov, E.N., Foh, J., Guetlich, P., Kankeleit, E., McCoy, T.J., Mittlefehldt, D.W., Renz, F., Schmidt, M.E., Zubkov, B., Squyres, S.W., Arvidson, R.E., Anonymous, 2006. Mössbauer mineralogy of rock, soil, and dust at Meridiani Planum, Mars; Opportunity's journey across sulfate-rich outcrop, basaltic sand and dust, and hematite lag deposits. J. Geophys. Res. 111.
Mozley, P., 1989. Complex compositional zonation in concretionary siderite; implications for geochemical studies. J. Sed. Petrol. 59, 815–818.
Mozley, P., Davis, J.M., 2005. Internal structure and mode of growth of elongate calcite concretions; evidence for small-scale, microbially induced, chemical heterogeneity in groundwater. Geol. Soc. Am. Bull. 117, 1400–1412.
Mozley, P., Goodwin, L.B., 1995. Patterns of cementation along a Cenozoic normal fault: a record of paleoflow orientations. Geology 23, 539–542.
Munsell Rock-Color Chart, 1975. Prepared by The Rock-Color Chart Committee, Distributed by The Geological Society of America, Boulder Colorado.
Ormo, J., Chan, M.A., Komatsu, G., Beitler, B., Parry, W., Souza-Egipsy, V., Boss, A., Meech, K., Thorsteinsson, T., 2004. Indications for microbial activity in the formation of hematite concretions in southern Utah; an analogue to the hematite deposits at the Opportunity landing site, Mars? Astrobiology 4, 283–284.
Ortoleva, P., 1994. Agates, geodes, concretions and orbicules; self-organized zoning and morphology. Fractals and Dynamic Systems in Geoscience. 283 pp.
Pantin, H.M., 1958. Rate of formation of a diagenetic calcareous concretion. J. Sed. Petrol. 28, 366–371.
Parrish, J.T., Falcon-Lang, H.J., 2007. Coniferous trees associated with interdune deposits in the Jurassic Navajo Sandstone Formation, Utah, USA. Palaeontology 50, 829–843.
Parry, W.T., Chan, M.A., Beitler, B., 2004. Chemical bleaching indicates episodes of fluid flow in deformation bands in sandstone. AAPG Bull. 88, 175–191.
S.L. Potter, M.A. Chan, Iron mass transfer and fluid flow patterns in Jurassic Navajo Sandstone, southern Utah, U.S.A., Geofluids submitted for publication.
Prosser, D.J., Daws, J.A., Fallick, A.E., Williams, B.P.J., 1994. The occurrence and delta (super 34) S of authigenic pyrite in Middle Jurassic Brent Group sediments. J. Pet. Geol 17, 407–428.
Raiswell, R., 1976. The microbiological formation of carbonate concretions in the upper Lias of NE England. Chem. Geol. 18, 227–244.
Raiswell, R., Fisher, Q.J., Cope, J.C.W., Curtis, C.D., 2000. Mudrock-hosted carbonate concretions; a review of growth mechanisms and their influence on chemical and isotopic composition. J. Geol. Soc. Lond. 157, 239–251.
Sefton-Nash, E., Catling, D., 2008. Hematitic concretions at Meridiani Planum, Mars; their growth timescale and possible relationship with iron sulfates. Earth Planet. Sci. Lett. 269, 365–375.
Seilacher, A., 2001. Concretion morphologies reflecting diagenetic and epigenetic pathways. Sed. Geol. 143, 41–57.
Seiler, W.M., 2008. Jurassic Navajo Sandstone of Coyote Buttes, Utah/Arizona: Coloration and Diagenetic History, Preservation of a Dinosaur Trample Surface, and a Terrestrial Analog to Mars. University of Utah.
Steefel, C.I., Van Cappellen, P., 1990. A new kinetic approach to modeling water–rock interaction; the role of nucleation, and Ostwald ripening. Geochim. Cosmochim. Acta 54, 2657–2677.
Squyres, S.W., Knoll, A.H., 2005. Sedimentary rocks at Meridiani Planum; origin, diagenesis, and implications for life on Mars. Earth Planet. Sci. Lett. 240, 1–10.
Stumm, W., Morgan, J.J., 1996. Aquatic Chemistry: Chemical Equilibria and Rates in Natural Waters. Wiley, New York. p. 1040.
Squyres, S.W., 2004. *In situ* evidence for an ancient aqueous environment at Meridiani Planum, Mars. Science 306, 1709–1714.
Squyres, S.W., 2009. Exploration of Victoria crater by the Mars rover Opportunity. Science 324, 1058–1061.
Tosca, N.J., McLennan, S.M., Clark, B.C., Grotzinger, J.P., Hurowitz, J.A., Knoll, A.H., Schroeder, C., Squyres, S.W., 2005. Geochemical modeling of evaporation processes on Mars; insight from the sedimentary record at Meridiani Planum. Earth Planet. Sci. Lett. 240, 122–148.